Processing of Copper by Keyhole-Gas Tungsten Arc Welding for Uniformity of Weld Bead Geometry

Raghavendra Darji[a], Vishvesh Badheka[a], Kush Mehta[a, b*], Jaydeep Joshi[c], Ashish Yadav[c]

[a]Department of Mechanical Engineering, School of Technology, Pandit Deendayal Petroleum University, Raisan, Gandhinagar.

[b]Advanced Manufacturing and Materials group, Department of Mechanical Engineering, School of Engineering, Aalto University, Espoo, Finland

[c] ITER-India, Institute of Plasma Research, Block A, Sangath Skyz IPL, Bhat, Ahmedabad.

[*]Corresponding author: kush_2312@yahoo.com, kush.mehta@aalto.fi

Abstract

Keyhole gas tungsten arc welding (K-GTAW) was applied to characterize the weld bead geometry in case of the 6 mm thick electrolytic tough pitch copper. Various conditions of welding speeds and the preheating on the bead on geometry were studied for uniformity of weld geometry. Visual examination, macro bead dimensional analysis, microhardness profile across the transverse section, microstructural analyses were performed to investigate the K-GTAW on electrolytic tough pitch copper. The results revealed that full penetration of 6 mm can be obtained in a single pass using keyhole mode in GTAW. Keyhole length and width were majorly affected by the welding speed and preheating temperature. Significant variations in weld bead geometry were observed even when high heat input conditions were applied without preheating. Uniform weld bead geometry of 5 mm bead width and depth to width ratio of 0.42 was obtained for a length of 80 mm using appropriate preheating of 300°C and heat input condition of 1.37 kJ/mm (resulted from 300 amps welding current, 120 mm/min welding speed and 15.3 volts voltage). In the uniform weld bead geometry, the weld and heat affected zones were consisted of coarse grains relative to base material, wherein the micro hardness variations were observed.

Keywords: Keyhole; GTAW; Copper; weld; bead; geometry; penetration; evaluation.

1. Introduction

Excellent thermal and electrical conductivities, corrosion resistance nature and extraordinary aesthetic appearance are unique features of copper (Cu) that attracts large number of applications in different sectors including households, shipbuilding, power, electrical, electronics and microelectronics, chemical, metallurgical automobile, manufacturing, petroleum, and nuclear [1-16]. Besides, the welding of the Cu is challenging due to higher thermal and electrical conductivities,

high melting point, hot short behavior, and high coefficient of thermal expansion [1–3]. Developments in welding approaches are being carried out to tackle these issues to obtain successful welds in Cu based alloys [17-20]. Preheating is one of such approaches known for enhanced welding of Cu especially for fusion based welding processes. It was observed that, the welding of Cu requires as high as 500 °C preheating temperature specifically when the thickness of Cu is higher than 3 mm [17]. Higher preheating leads to produce coarse grains in the weld zone and heat affected zone (HAZ). It was also prone to form defects such as porosity and the cracking tendency of the Cu during bead on plate (BOP) study, as reported in case of laser arc hybrid welding [17]. The weld metal ejection was an another issue observed in laser arc hybrid welding [2]. However, other literature of [21] depict that laser welding in vacuum was more stabilized, wherein the formation of porosities was considerably suppressed with an application of welding speed in between 0.5 to 2 m/min. In case of gas tungsten arc welding (GTAW) of Cu studied by, [22] it was observed that the welds were consisted micro cracking that was observed due to longer time in critical crystalline range during the solidification along with high amount of the oxygen in the weld metal. This issue is susceptible in GTAW of Cu.

Despite of great interest in welding of Cu with it's afore mentioned challenges, limited articles are available in this domain. Majority of the articles are on laser welding [18] and solid state welding processes [1,23], wherein many issues are yet to be resolved. To the best of authors' opinion, there is no article available that addresses issues on uniformity of weld bead across the length when subjected by GTAW process. The keyhole mode of GTAW for the analysis of Cu welding and bead on geometry was never attempted in previous literature. It is worth to analyses K-GTAW on Cu welding as higher welding current can be employed that is used to promote the arc force, which in turn increases penetration depth of weld bead [24-26]. This investigation was carried out to establish

uniform weld bead using keyhole GTAW for Cu for the application of hydraulic grid in the diagnostic neutral beam of International Thermonuclear Experimental Reactor (ITER).

2. Materials and Methods

Commercially pure electrolytic tough pitch copper (ETP Cu) of 100 X 50 X 6 mm was used in this experimental investigation (refer Table 1 for the chemical compositions). The experiments were performed on the set up shown in Fig. 1, with constant process parameters as mentioned in Table 2. Also, other conditions such as backing plate, type of shielding gas, and power source characteristics were kept constant as carbon steel, commercially pure argon (of grade II), and constant current respectively. High heat input capacity power source with current caring capacity up to of 500 amperes was utilized in this experimental investigation. There were six number of experiments performed (from T1 to T6) with various conditions as shown in Table 3.

Welding speed, preheating conditions and current were varied during the experiments, in order to change the heat input conditions and cooling rate effects. The selection of process parameters was carried out based on visual inspection during and after experiments. GTAW torch was used for preheating application at the location of start. The intended preheat temperature as mentioned in Table 3 was obtained using this GTAW torch at the start of weld without moving the torch. Fluke 62MAX, non-contact type infrared thermometer was used to measure the preheating temperatures. Preheating temperatures were measured from 1 feet distance at mid length of the specimen, at 50 mm length and 10 mm away from the weld center line. As soon as desired preheat temperature arrives, the welding phase was conducted. The variations in parameters were carried out based on visual examination and the heat input conditions observed after each experiment. The heat input

conditions were examined using (1) (adopted from [27-29]) and subsequently travel speed, current and application of preheating with different temperatures were varied.

$$Heat\ Input = \eta \times \frac{60\ X\ V \times I}{1000\ X\ s}, \quad (1)$$

where, I is the welding current, V is the voltage and S is the welding speed (defines the arc energy with multiplication factor 0.06) and η is the process efficiency, presumed 0.6 based on [29].

The visual examination was performed on surface of welds from the face and root sides. The uniformity on bead on weld was evaluated across the length with weld bead measurements as shown in the Fig. 2 (at three distinct regions, such as 5 mm from the start of the weld, 20 mm before the end of weld and mid length in the transverse direction). The mid length variations were further measured at every 15 mm.

After the dimensional measurements, all the samples were extracted from the cross section, in order to perform macro examination. Each of these samples was extracted from the same location of 20 mm before the end portion of the welds (considering the comparison on wider keyhole). The samples were further prepared using standard metallographic procedure. The rough grinding followed by the fine grinding of 1/0, 2/0, 3/0 and 4/0 grinding papers were performed as a first step of metallography. Polishing was performed using slurry of water and alumina powder after the grinding phase. The samples were etched using potassium dichromate by cotton cloth as a last stage of metallography. The depth-to-width (D/W) ratio was calculated during the macro examination using stereomicroscope (BSA A model) of Benbros Engineering. Based on results, the sample resulted with uniform weld bead geometry was subjected to microstructure and microhardness profile. Microstructural features were investigated using the optical microscopy and energy dispersive

spectroscopy. Microhardness measurements were carried out using 100 grams of load applied for 10 seconds at each 1 mm interval across the width of the specimen.

3. Result and Discussion

The surface appearances of the bead on profile from face and root sides are shown in Fig. 3 that revealed no surface defects. The defects such as spatters and humps are commonly observed in case of welding of Cu due to weld metal ejection phenomenon in case of fusion based welding [2,21]. However, the bead profiles were non-uniform across the length of each specimen. It can be seen that the width was narrow at the beginning (i.e. start position) and increases with a progress of length (hence completes with maximum bead width). This phenomenon is due to higher conductivity of Cu base material. In the beginning of weld, the heat was conducted quickly in the bulk of Cu and that subsequently dissipates rapidly due to higher thermal conductivity of Cu that in turn obstacles the conditions for keyhole formation. As soon as the GTAW torch travels across the intended length, effect of keyhole was obtained in Cu after reaching to favorable heating conditions. This condition of keyhole was obtained at different length due to district parametric conditions. Full penetration level of 6 mm can be seen at the root side, wherein full keyhole mode of GTAW process was revealed. The length of obtaining keyhole condition was distinct in all the experiments as different parametric conditions were subjected. Fig. 4 shows keyhole obtained under different conditions. The maximum keyhole length was obtained for conditions T3 and T5 wherein highest length of penetration of 80 mm was obtained. Both of these conditions were performed with preheating. However, the weld bead shape was district across the length in these two conditions.

Fig. 5 shows dimensional analysis on weld bead width (of face side) across the length under different conditions of Table 3. Maximum variation from 3 mm to 29 mm in bead width was

observed in T1 condition, whereas minimum variation from 10 mm to 16 mm was observed with T5 condition. The imbalance between heat input and heat conduction influences width of weld bead across the length of Cu workpiece. The weld bead variation was largely non-uniform with the conditions of no preheating (i.e. T1 and T2) even though the high heat input conditions (refer Table 4) were subjected. These variations were significant when specimen was not preheated initially before experimentation due to higher temperature gradient. This may be the strongest reason for huge variations in bead width and keyhole length in case of T1 and T2 conditions. The keyhole length obtained in case of T1 was 65 mm, however, the bead width variation was too large due to the very slow welding speed of 60 mm/min. These variations in bead width were reduced with an increase in the welding speed of 90 mm/min, however, the keyhole length was reduced to 38 mm, in case of T2 condition.

Besides, the improvements in uniformity of weld bead geometry and penetration level were obtained with preheating condition. Condition of T3 (with preheating of 250°C) was resulted in improved penetration compared to condition of T2 (without preheating) at same process parameters (i.e. 1.82 kJ/mm heat input (refer Table 4) with 300 amp current and 90 mm/min travel speed). Condition T5 (with preheating of 300°C and heat input of 1.37 kJ/mm (refer Table 4)) was resulted in most uniform weld bead geometry from face and root side compare to all conditions mentioned in Table 3.

Due to the results obtained after T5 experiment, it can be concluded that 300 ^{0}C preheating and the 120 mm/min welding speed with 300 amperes welding current were suitable parameters for the keyhole GTAW of ETP Cu for dimensions of 100 X 50 X 6 mm. The preheating employed for the T5 experiment that produced the uniform bead (as can be seen from Fig. 6) was high as compare to the other experiments in which preheating temperatures were low.

In experiments of T3 and T4 conditions, variations obtained in the bead width were 24 mm and 14 mm with the keyhole length of 82 mm and 42 mm respectively. T3 and T4 were performed using 90 mm/min and 120 mm/min welding speeds respectively along with preheating of 250 ^{0}C. T3 was performed with similar process parameters of T2 having only difference on preheating. As a result, during the bead on plate run more amount of heat was utilized to produce the keyhole mode. Even though, the heat conducted along the width of the specimen resulted into the highest variations in the bead width. It can be interpreted that the welding speed was slower that served as additional preheating source and subsequently resulted in wider keyhole across the progressing length. In case of preheating condition, the heat conduction was possible along the width of the base metal that can help in stabilization of keyhole. Preheating was applied using welding torch using dwell time at the start of process. The transverse movement was applied when desired preheating temperature has reached. The bead width of T3 was the widest at the end portion of weld bead among all the experiments as shown in Fig. 7, which was resulted with large variations. Therefore, experimental condition of T4 was executed with the higher welding speed of 120 mm/min in order to reduce the variation in the bead width using lower heat input (refer Table 4) relative to T3 condition. The higher welding speed dwindled the variations in the bead width; however, the keyhole length was also reduced to considerable extent compare to T3 weld bead. The results obtained after these experiments revealed that slower welding speed degrade the characteristics of the bead width at the same time higher welding speed keeping the preheating temperature constant reduced the keyhole length. This affirms that the preheating condition needs to be increased so that proper keyhole conditions can be obtained. Therefore, the preheating temperature was raised to the 300 ^{0}C while keeping the welding speed constant in case of T5 condition. With T5 condition, uniform keyhole mode was maintained for larger length that subsequently resulted in uniform weld bead across 80

mm length of the specimen. The set of parameters of T5 condition was resulted into a heat input value of 1.37 kJ/mm (refer Table 4). In order to reduce the heat input, T6 experiment was conducted with 275 amperes welding current keeping rest parameters constant relative to T5 condition. However, the variation in the bead width was less and near to bead width variation of T5, whereas the keyhole length was reduced to 30 mm. The reduction of keyhole length was significantly influenced by heat input that was reduced to 1.17 kJ/mm (refer Table 4) due to decreased current of 275 amperes. Taking heat input values into consideration from the table 4, it can be observed for the present investigation that, the favorable heat input value was 1.37 kJ/mm along with the 300 ^{0}C preheating temperature. Other than experiment T5, all other heat input values were not favorable with the consideration of bead geometry, higher heat input values (caused in experiment T1 to T3) showed the excessively wider beads (with decreased the D/W ratio) and lower heat input (T6) resulted into the shorter keyhole length.

Fig. 8 shows the cross-sectional macro examinations of bead on plate for aforementioned conditions of T1 to T6. Full penetration of Fig. 8 was not remained throughout the length of the specimen as discussed in section 3.1 and hence, best penetration condition was presented from each case. It can be seen that the macrographs were defect free without any voids and porosity. Besides, Miyagi and Zhang [30] observed porosity and voids in the macrographs of laser beam welded Cu due to the capillary behavior and weld metal ejection. The keyhole mode of GTAW was a strong possible reason behind the defect free welds. In case of GTAW the formation of the keyhole was wider due to the bell shape arc as compare to LBW (Laser Beam Welding) [21], which in turn helped in proper shielding with improved fluidity of Cu in weld pool. Therefore, defect free macrographs were resulted in all the conditions wherein full keyhole mode was obtained. It can also be observed that the keyhole shape that was distinct for each condition has influenced shape of the weld bead

geometry. The weld bead at the bottom was wide in case of T1 and T3, moderate for T2 and T4, and narrow for T5 and T6. The reinforcement was not present while full penetration was present due to keyhole effect in all the cases.

Fig. 9 shows the depth-to-width (D/W) ratio measured after the macro examination under the effect of keyhole. Higher D/W ratio for the conditions of T2, T4, T5 and T6 was observed, wherein highest D/W ratio of 0.42 was obtained with T5 condition that resulted from narrow width of keyhole. This was reported even higher as compared to published literature of Cheng et. al [31] wherein maximum D/W ratio was 0.34 observed with red-Cu using the argon and nitrogen gas mixture in GTAW without preheating. Besides, in other cases, due to the wider keyhole, the D/W ratios were low as compare to T5. However, the D/W ratios observed with T4 and T6 were very close to T5 but not uniform throughout the length. As mentioned in above sections, the non-uniform heat conduction was a problem for variation in keyhole uniformity that subsequently influenced the uniformity of keyhole throughout the length.

The microhardness profile measured from the transverse cross section of T5 weld bead is shown in Fig. 10. There were no major variations observed in the microhardness of the weld, HAZ and parent metal. The hardness profile obtained in the weld region was ranging between 44 to 50 $HV_{0.1}$, which was similar in the HAZ too. Whereas, the base metal shows the hardness in between 55 to 60 $HV_{0.1}$. In this condition of T5, 1.37 kJ/mm heat input (refer Table 4) was employed along with the preheating temperature of 300 ^{0}C, which in turn resulted in the slow rate of cooling of 3.31 ^{0}C/second as confirmed by time-temperature graph shown in Fig. 11. Due to slow cooling rate, the softening mechanism turn to be dominant and subsequently responsible for grain coarsening effect that may have led to low microhardness [32]. Microstructural analysis was performed to understand grain coarsening effect in support of microhardness variations.

Fig. 12 shows the microstructures of T5 specimen from various locations such as weld, HAZ and parent metal. The grain coarsening can be confirmed in weld and HAZ regions, which was responsible for low hardness as compared to parent material. Additionally, small size round shaped particles were noticed in microstructures of weld [Fig. 12 (a)-(b)] and HAZ [Fig. 12 (c)-(d)]. These particles may have formed with composition of cuprous oxides considering susceptible reaction of Cu with oxygen. It is reported that cuprous oxides are prone to cause cracks in the weld zone in case of the Cu welding. Cuprous oxides can act as a eutectic, which are also known for the formation of liquid film in between solidified grains, and ultimately torn due to the shrinkage and stress at the grain boundaries that results in cracks [22]. However, in the present study, no such cracking effect was noticed in the microstructures. Application of 100 % argon as a shielding gas may have protected excess interaction of oxygen with Cu that may have resulted in defect free weld. In case of Yinan et al. [22], helium was used as shielding gas for GTAW of Cu. Furthermore, it can be seen from Fig. 12 that the crystal twining was observed in parent metal and HAZ that was expected due to wrought alloy [33].

Energy dispersive spectroscopy (EDS) was performed to identify the presence of cuprous oxide in the weld zone produced with T5 condition. Fig. 13(a) shows image of scanning electron microscopy in weld zone and condition. Fig. 13(b) shows spectrum of EDS performed on spot shown in Fig. 13(a). It can be seen that 18.32 atomic % of oxygen was noticed with rest of Cu. This was observed as presence of cuprous oxide particles in weld zone distributed in random manner however mostly inside the grains. It was observed that cuprous oxide with 28 atomic % of oxygen can lead to crack formation in case of Yinan et al. [22]. This may be the reason for defect free weld zone at macro and micro levels wherein formation of cuprous oxide was restricted with 18.32 atomic % of oxygen.

4. Conclusions

The study was performed to understand the behavior of keyhole gas tungsten arc welding (K-GTAW) mode on electrolytic tough pitch copper (ETP-Cu) for its bead on plate analysis under different conditions. Successful bead on plate analysis was carried out. Following specific conclusions can be made from this investigation.

1) K-GTAW was implemented on 6 mm thick the ETP-Cu with defect free bead on geometries under all investigated preheating conditions and heat inputs.
2) Depth of keyhole was majorly influenced by the welding speed, welding current and the preheating temperature for the K-GTAW of Cu. Keyhole length and width were affected by the welding speed and preheating temperature.
3) Preheating governs uniformity of the keyhole in K-GTAW of Cu.
4) Uniform bead on plate geometry with depth to width ratio of 0.42 was obtained for 80 mm of length, under T5 condition of 300 amperes of welding current, 120 mm/min of welding speed and 300^0C of preheating temperature, where in heat input condition was 1.37 kJ/mm.
5) Minor variations in microhardness was observed in the weld and HAZ (44 to 50 $HV_{0.1}$) compared to base metal (55 to 60 $HV_{0.1}$), under T5 condition.
6) Coarse grains were observed in the weld and HAZ. The HAZ grains were coarse equiaxed with twins while the base metal also consisted of finer equiaxed grains with the twins, under T5 condition.
7) In under T5 condition, the microstructures of weld were consisted cuprous oxides (even though resulted in defect free weld) as revealed in the SEM-EDS analysis.

Acknowledgments

The authors would like to acknowledge the funding support of Board of Research in Nuclear Sciences (BRNS) from project no.39/14/04/2018-BRNS.

References

[1] Sun, Y. F.; Fuji, H. Investigation of the welding parameter dependent microstructure and mechanical properties of friction stir welded pure copper. *Mater. Sci. Eng. A*. **2010**, 527, 6879–6886. DOI: 10.1016/j.msea.2010.07.030.

[2] Wang, L.; Li, X.; Gao, M.; Zeng, X. Stabilization mechanism and weld morphological features of fiber laser-arc hybrid welding of pure copper. *J. Manuf. Process.* **2017**, 27, 207–213. DOI: 10.1016/j.jmapro.2017.05.009.

[3] Butterworth , G. J.; Forty, C. B. A. A survey of the properties of copper alloys for use as fusion reactor materials *J. of nucl. mat*. **1992**, 189, 237–276. DOI: 10.1016/0022-3115(92)90381-T**.**

[4] Mehta, K. P.; Badheka, V. J. Influence of tool pin design on properties of dissimilar copper to aluminum friction stir welding. *Trans. Nonferrous Met. Soc. China*. **2017**, 27, 36 - 54. DOI: 10.1016/S1003-6326(17)60005-0.

[5] Mehta, K. P.; Badheka, V. J. A review on dissimilar friction stir welding of copper to aluminum: Process, properties, and variants. *Mater. Manuf. Process.* **2016**, 31, 37-41. DOI: 10.1080/10426914.2015.1025971.

[6] Mehta, K. P.; Badheka,V. J. Effects of tilt angle on the properties of dissimilar friction stir welding copper to aluminum. *Mater. Manuf. Process.* **2016**, 31, 255 - 263. DOI: 10.1080/10426914.2014.994754.

[7] Teng, Y. L.; Li, L.; Zhang, W.; Wang, N.; Feng, C. C.; Ren, J. H. Machining characteristics of PCD by EDM with Cu-Ni composite electrode. *Mater. Manuf. Process.* **2020**, 35, 442–448. DOI: 10.1080/10426914.2020.1718700.

[8] Tang, D.; Li, J.; Wang, L.; Wang, Z.; Kong, C.; Yu, H. Fabrication of gradient-structure CuNiBe alloy bars by laser remelting and water-cooling. *Mater. Manuf. Process*. **2020**, 35, 337–345. DOI: 10.1080/10426914.2020.1726948.

[9] Guo, W.; Yi, Y.; Huang, S.; Mao, X.; Fang, J,; Tong, D.; Luan, Y. Manufacturing large 2219 Al–Cu alloy rings by a cold rolling process. *Mater. Manuf. Process*. **2020**, 35, 291–302. DOI: 10.1080/10426914.2020.1718696.

[10] Annuar, N. S. M.; Mahmoodian, R.; Shukor, M. H. A. Effect of focused ion beam process parameter on Tin-Nickel-Copper micropillars microfabrication. *Mater. Manuf. Process*. **2020**, 35, 163–171. DOI: 10.1080/10426914.2020.1711923.

[11] Aghbolagh, V. M.; Alimirzaloo, V.; Khamedi, R. Constrained groove pressing process of Al/Cu bimetal sheet. *Mater. Manuf. Process*. **2020**, 35, 130–141,DOI: 10.1080/10426914.2019.1692351.

[12] Gao, P.; Zhang, Y.; Mehta, K.P. Metallurgical and Mechanical Properties of Al–Cu Joint by Friction Stir Spot Welding and Modified Friction Stir Clinching. *Met. Mater. Int.* **2020**, DOI: 10.1007/s12540-020-00759-w.

[13] Carvalho, G. H. S. F. L.; Galvão, I.; Mendes, R.; Leal, R. M.; Loureiro, A. Friction stir welding and explosive welding of aluminum/copper: process analysis. *Mater. Manuf. Process.***2019**, 34,1243–1250. DOI: 10.1080/10426914.2019.1644452.

[14] Jiang, W.; Guan, F.; Li, G.; Jiang, H.; Zhu, J.; Fan, Z. Processing of Al/Cu bimetal via a novel compound casting method. *Mater. Manuf. Process.* **2019**, 34, 1016–1025. DOI: 10.1080/10426914.2019.1615084.

[15] Joshi, G. R.; Badheka, V. J. Processing of bimetallic steel-copper joint by laser beam welding. *Mater. Manuf. Process.***2019**, 34, 11, 1232–1242. DOI: 10.1080/10426914.2019.1628262.

[16] Shahid, M. B.; Han, S. C.; Jun, T. S.; Park, D. S. Effect of process parameters on the joint strength in ultrasonic welding of Cu and Ni foils. *Mater. Manuf. Process.* **2019**, 34, 1217–1224. DOI: 10.1080/10426914.2019.1643474

[17] Zhang, L. J.; Ning, J.; Zhang, X. J.; Zhang,G. F.; Zhang, J. X. Single pass hybrid laser-MIG welding of 4-mm thick copper without preheating. *Mater. Des.* **2015**, 74, 1–18. DOI: 10.1016/j.matdes.2015.02.027.

[18] Auwal, S. T.; Ramesh, S.; Yusof, F.; Manladan, S. M. A review on laser beam welding of copper alloys. *Int. J. Adv. Manuf. Technol.* **2018**, 96, 475-490. DOI: 10.1007/s00170-017-1566-5.

[19] Mehta, K. P.; Badheka, V. J. Hybrid approaches of assisted heating and cooling for friction stir welding of copper to aluminum joints. *J. Mater. Process. Technol.* **2017**, 239, 336–345. DOI: 10.1016/j.jmatprotec.2016.08.037.

[20] Mehta, K.; Gupta, K. Advanced Joining and Welding Techniques: An overview. *Adv. Manuf. Technol. Mater. Form. Machi. and Trib.* **2017**, 101–136. DOI: 10.1007/978-3-319-56099-1.

[21] Reisgen, U.; Olschok, S.; Jakobs, S.; Turner, C. Sound welding of copper: Laser beam welding in Vacuum. *Phys. Procedia*. **2016**, 83, 447–454. DOI: 10.1016/j.phpro.2016.08.046.

[22] Yinan, L.; Shanbin, Z.; Zilong, P.; Feng, G. A Study on the Mechanism of Crystal Cracking in GTA Welding of Copper Plates. *Mater. Manuf. Process.* **2016**, 31, 2143–2151. DOI: 10.1080/10426914.2015.1103861.

[23] Nakata, K. Friction stir welding of copper alloys. *Weld. Int.* **2005**, 19, 929–933. DOI: 10.1533/wint.2005.3519.

[24] Fan, W. ; Ao, S.; Huang, Y.;Liu, W.; Li, Y.; Feng, Y.; Water cooling keyhole gas tungsten arc welding of HSLA steel . *Int. J. Adv. Manuf. Technol.* **2017**, 92, 2207-2216. DOI: 10.1007/s00170-017-0234-0.

[25] Fei, Z.; Pan, Z.; Cuiuri, D.; Li, H.; Gazder, A. A. A combination of keyhole GTAW with a trapezoidal interlayer: A new insight into armour steel welding. *Materials (Basel).***2019**, 12, 1–18. DOI: 10.3390/ma12213571.

[26] Liu, S.; Liu, Z. M.; Zhao, X. C.; Fan, X. G. Influence of cusp magnetic field configuration on K-TIG welding arc penetration behavior. *J. Manuf. Process.* **2020,** 53, 229–237, DOI: 10.1016/j.jmapro.2020.02.027.

[27] Aval, H. J.; Farzadi, A.; Serajzadeh, S. Theoretical and experimental study of microstructures and weld pool geometry during GTAW of 304 stainless steel. I*nter. j. Adv.Manuf. Technol.* **2009**, 42, 1043–1051. DOI: 10.1007/s00170-008-1663-6.

[28] Sharma, P.; Dwivedi, D. K. Comparative study of activated flux-GTAW and multipass-

GTAW dissimilar P92 steel-304H ASS joints. *Mater. Manuf. Process.* **2019**, 34, 1–10, DOI: 10.1080/10426914.2019.1605175.

[29] The Welding Institute. TWI Limited https://www.twi-global.com/technicalknowledge/faqs/faq-what-is-the-difference-between-heat-input-and-arc-energy. (Accessed May 11, 2020).

[30] Miyagi, M.; Zhang, X. Investigation of laser welding phenomena of pure copper by x-ray observation system. *J. Laser Appl.* **2015**, 27, 042005, DOI: 10.2351/1.4927609.

[31] Lei, Y. C.; Yu, W. X.; Li, C. H.; Cheng, X. N. Simulation on temperature field of TIG welding of copper without preheating. *Trans. Nonferrous Met. Soc. China* . **2006,** 16, 838–842, DOI: 10.1016/S1003-6326(06)60336-1.

[32] Lin, J. W.; Chang, H. C.; Wu, M. H. Comparison of mechanical properties of pure copper welded using friction stir welding and tungsten inert gas welding. *J. Manuf. Process.* **2014**, 16, 296–304, DOI: 10.1016/j.jmapro.2013.09.006.

[33] Davis, J. R.; Copper and Copper Alloys, ASM Speciality Handbook , **2001,**32-33.

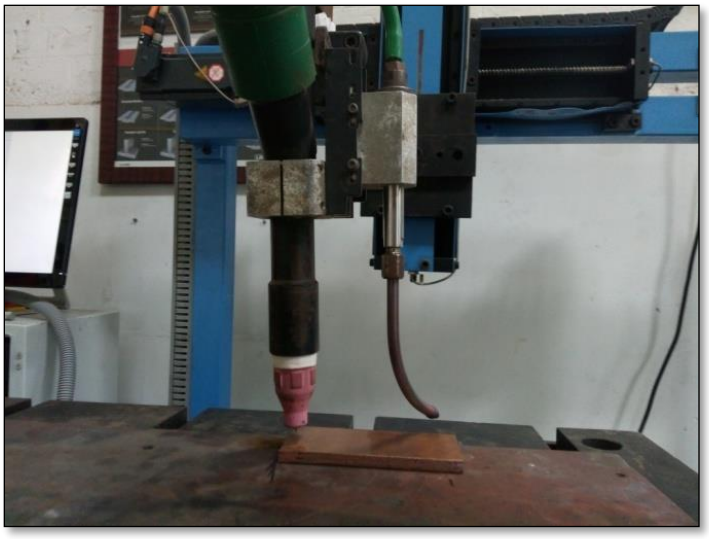

Figure 1. Experimental set up used to conduct the experiments.

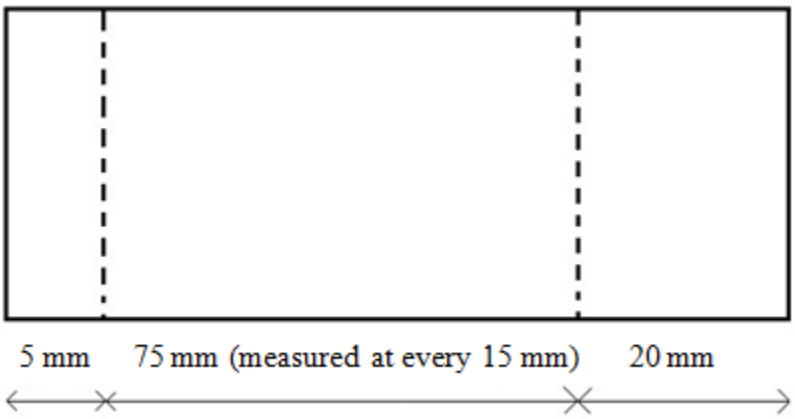

Figure 2. Locations for bead dimension analysis

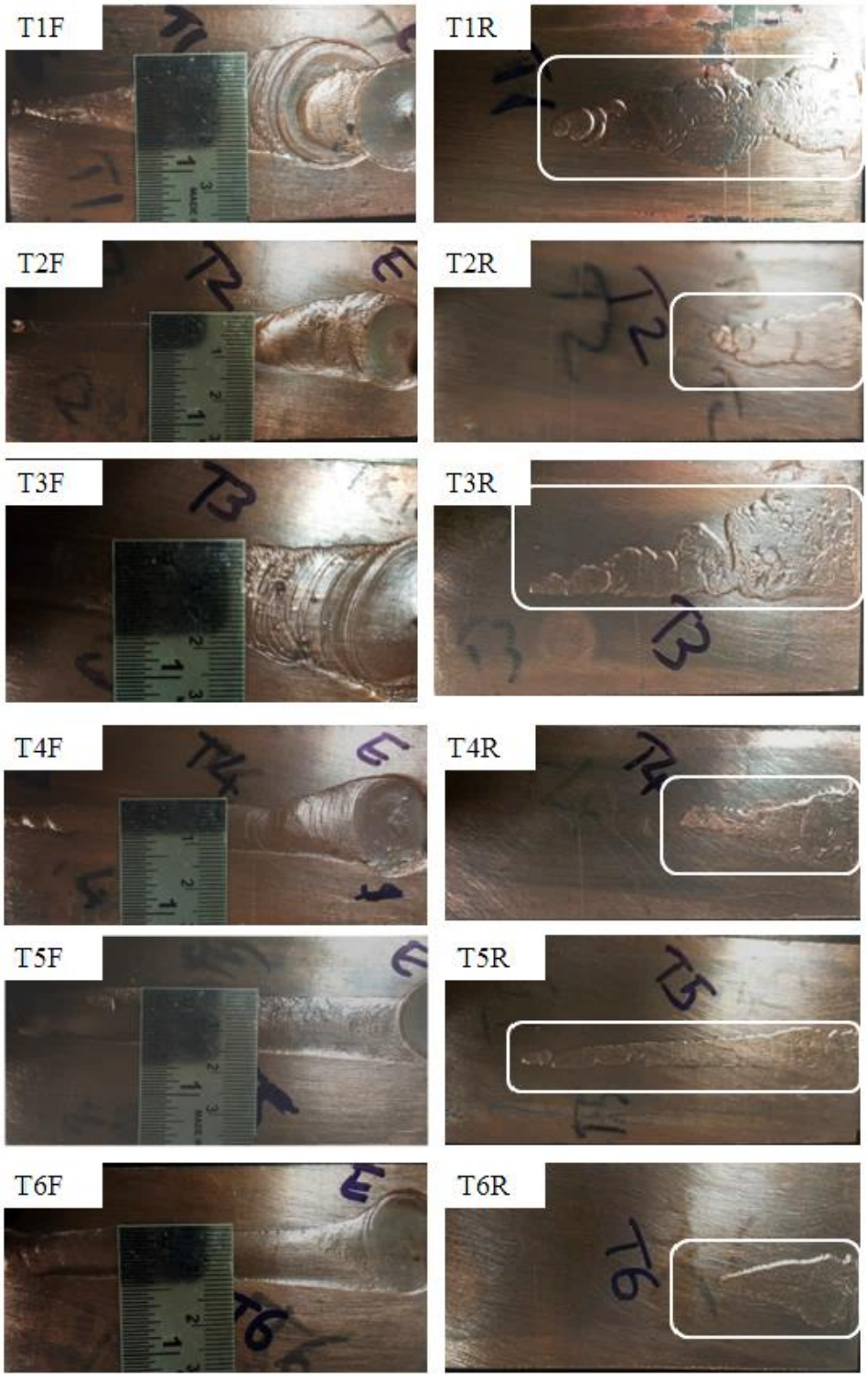

Figure 3. Visual appearance from face and root sides of the weld; (Suffix F and R indicate the face side and root side respectively)

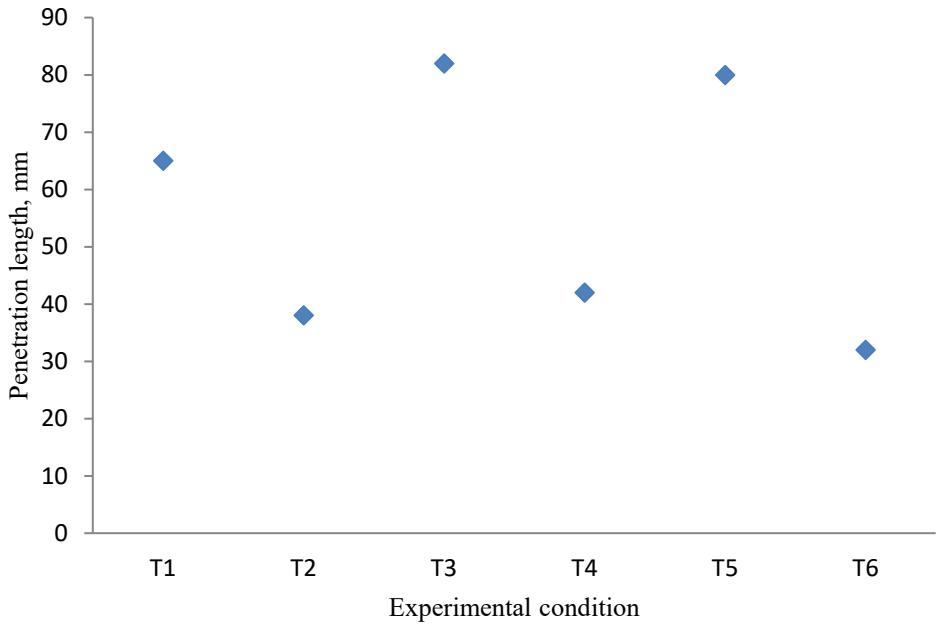

Figure 4. Keyhole length obtained under different experimental conditions.

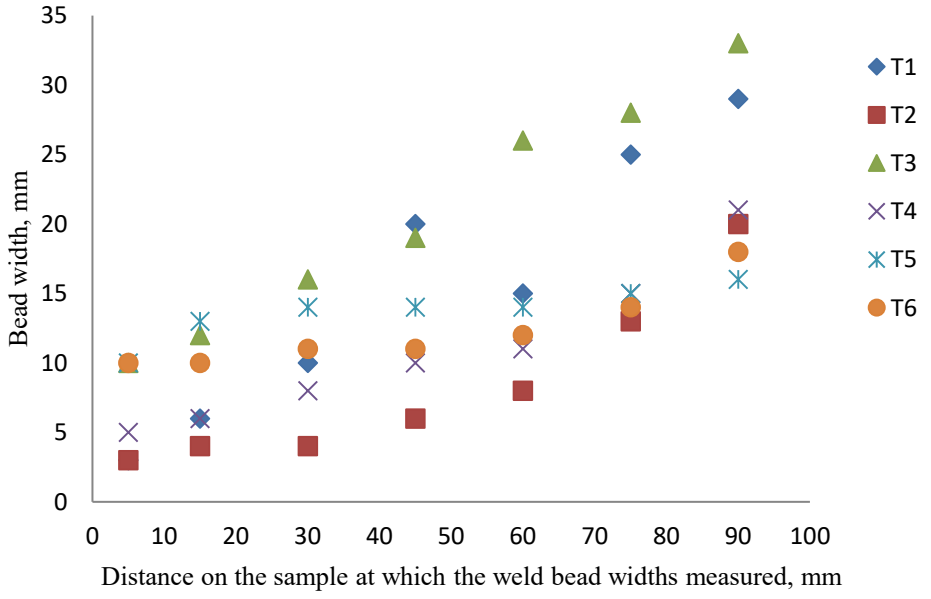

Figure 5. Variations in the bead widths.

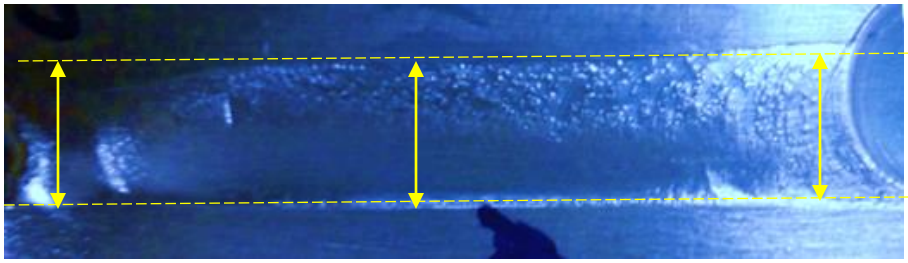

Figure 6. Bead width uniformity obtained in T5 condition

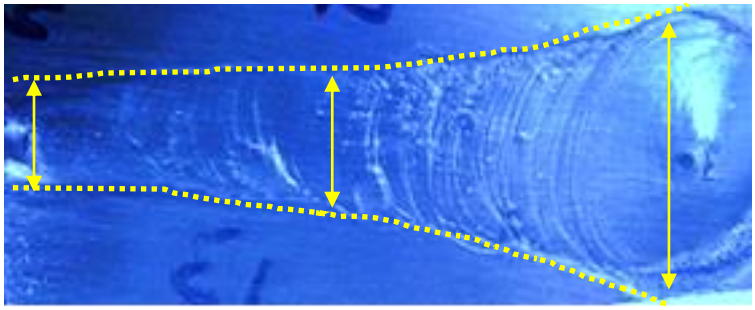

Figure 7. Bead shape in case of T3 condition

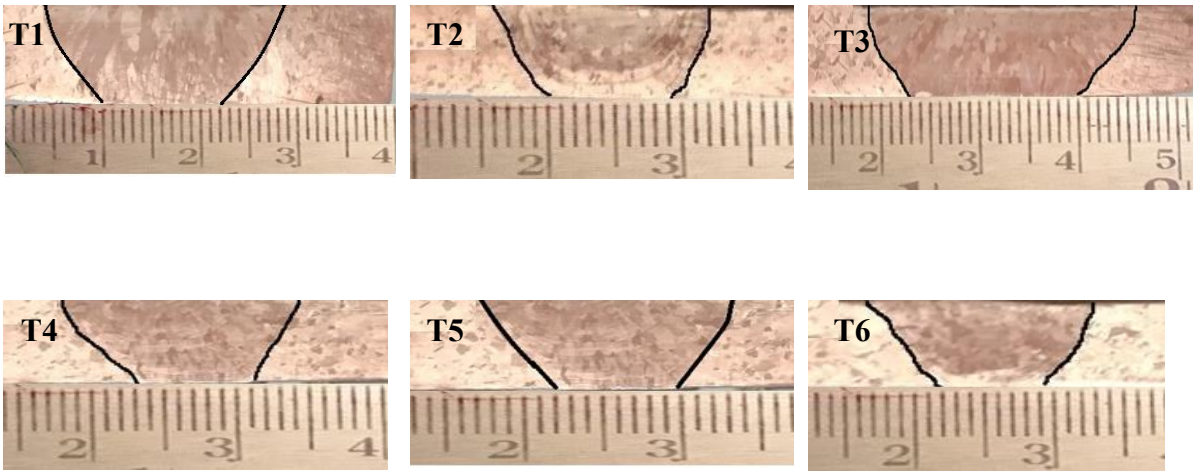

Figure 8. Macro examination under the effect of keyhole

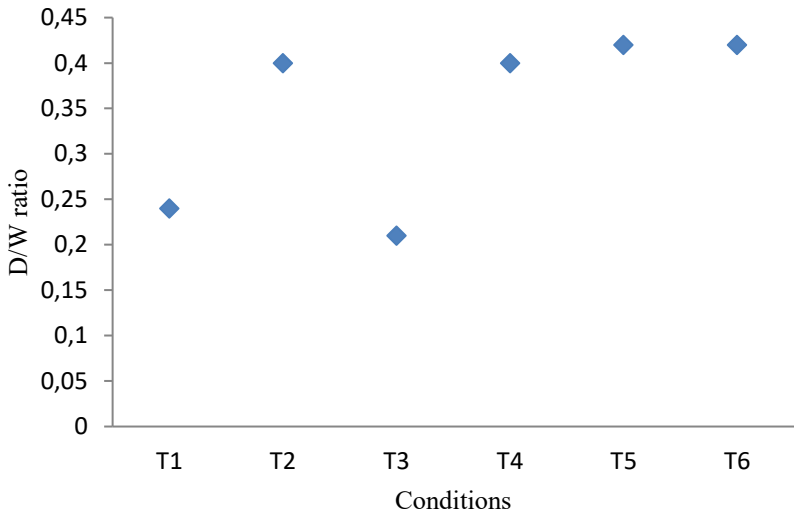

Figure 9. D/W ratio results (measured considering the average bead width across the length of obtained keyhole).

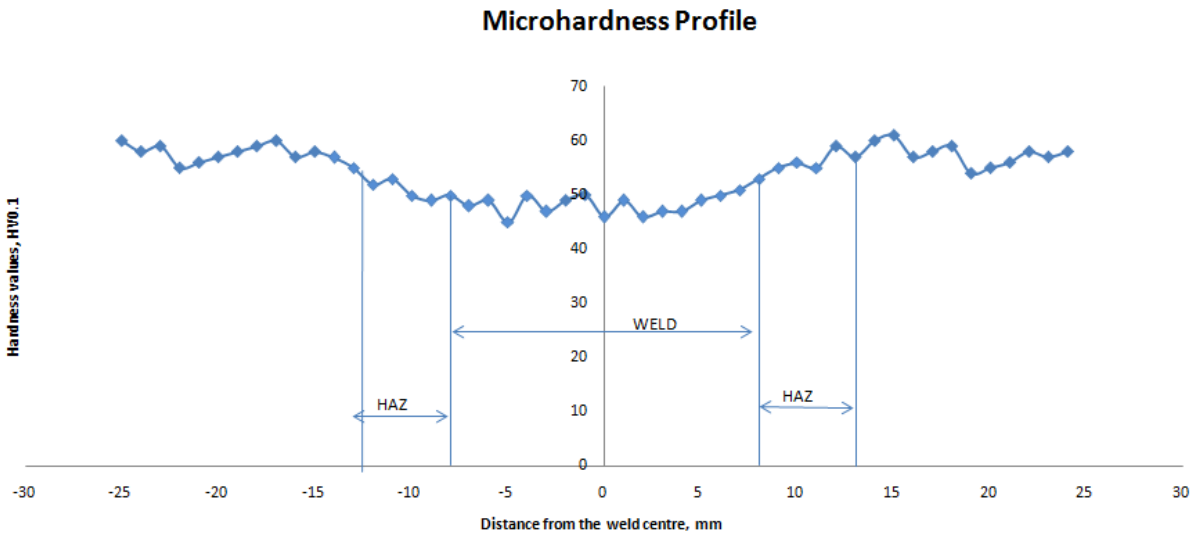

Figure 10. Microhardness profile obtained with the T5 sample.

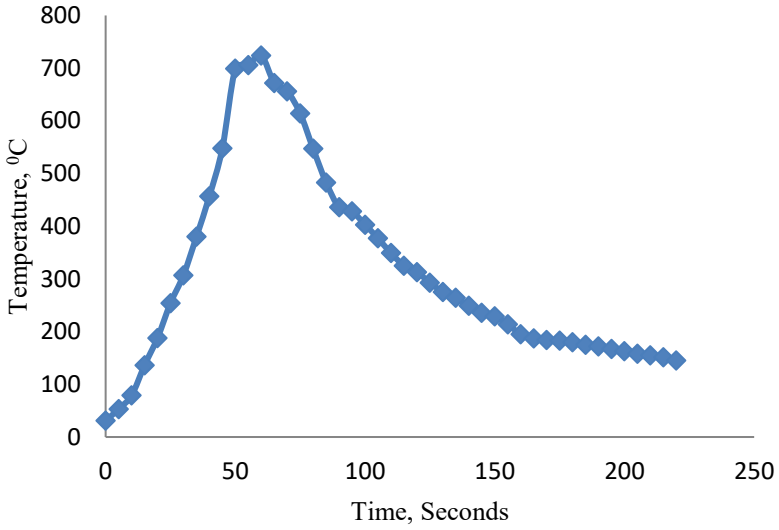

Figure 11. Temperature profile (rate of heating and cooling) obtained for the experiment T5.

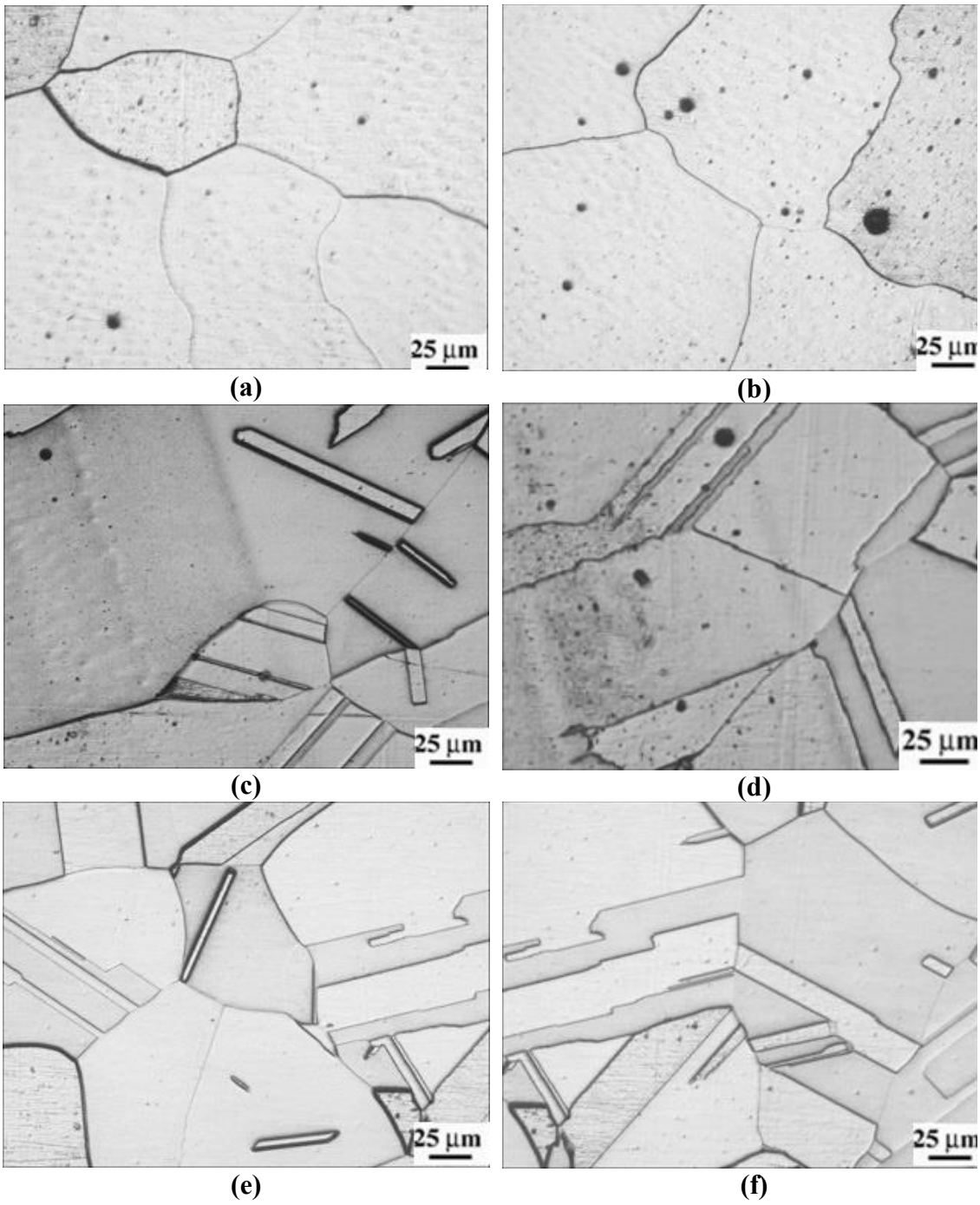

Figure 12. Microstructures of T5 condition; **(a)-(b)** weld, **(c)-(d)** HAZ and **(e)-(f)** parent metal

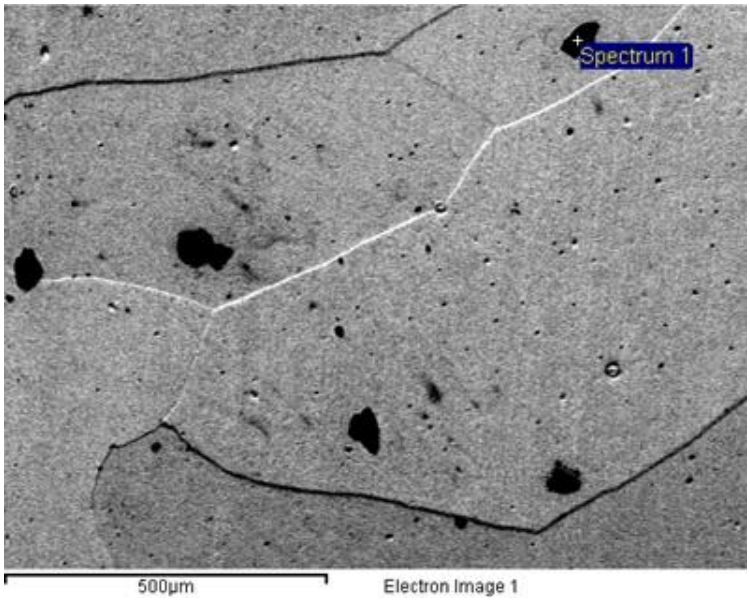

(a)

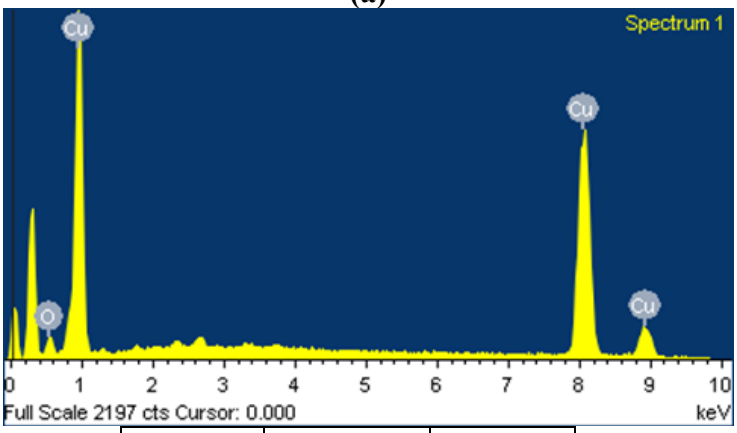

elements	weight %	atomic %
O K	5.34	18.32
Cu K	94.66	81.68
totals	100	

(b)

Figure 13 (a) Image of scanning electron microscopy in weld zone and **(b)** energy dispersive spectroscopy results of spot mentioned in **(a).**

Table 1. Chemical compositions of ETP copper.

Element	Copper	Lead	Phosphorous	Silicon
Amount in (%)	99.988	0.002	0.005	0.005

Table 2. Constant process parameters of the investigation

Sr No.	1	2	3	4	5
Parameters	Tungsten to Work piece distance (mm)	Gas Flow rate(l/min)	Electrode type	Electrode diameter (mm)	Angle of Tip (Degree)
Values / Specification	2	15	EWLa - 2	3.2	25

Table 3. Different process parameters and conditions of the investigation

Parameters / Sample Id	Current (Amperes)	Voltage (Voltage)	Welding Speed (mm/min)	Preheating conditions/Temperature
T1	300	15.3	60	No preheating
T2	300	15.2	90	No preheating
T3	300	15.3	90	250^0 C
T4	300	14.8	120	250^0 C
T5	300	15.3	120	300^0 C
T6	275	14.2	120	300^0 C

Table 4. Heat input under different conditions

Experiments	T1	T2	T3	T4	T5	T6
Heat Input (kJ/mm)	2.75	1.82	1.83	1.33	1.37	1.17